Journal of Saudi Chemical Society (2021) **25**, 101367

King Saud University

Journal of Saudi Chemical Society

www.ksu.edu.sa
www.sciencedirect.com

ORIGINAL ARTICLE

In silico studies on phytochemicals to combat the emerging COVID-19 infection

Mohnad Abdalla [a], Ranjan K. Mohapatra [b,*], Ashish K. Sarangi [c], Pranab K. Mohapatra [d], Wafa Ali Eltayb [e], Mahboob Alam [f,*], Amr Ahmed El-Arabey [f], Mohammad Azam [h,*], Saud I. Al-Resayes [g], Veronique Seidel [i,*], Kuldeep Dhama [j]

[a] *Key Laboratory of Chemical Biology (Ministry of Education), Department of Pharmaceutics, School of Pharmaceutical Sciences, Cheeloo College of Medicine, Shandong University, 44 Cultural West Road, Shandong Province 250012, PR China*
[b] *Department of Chemistry, Government College of Engineering, Keonjhar, Odisha 758002, India*
[c] *Department of Chemistry, School of Applied Sciences, Centurion University of Technology and Management, Odisha, India*
[d] *Department of Chemistry, C. V. Raman Global University, Bidyanagar, Mahura, Janla, Bhubaneswar, Odisha 752054, India*
[e] *Biotechnology Department, Faculty of Science and Technology, Shendi University, Shendi, Nher Anile, Sudan*
[f] *Division of Chemistry and Biotechnology, Dongguk University, 123 Dongdae-ro, Gyeongju, Republic of Korea*
[g] *Department of Pharmacology and Toxicology, Faculty of Pharmacy, Al-Azhar University, Cairo, Egypt*
[h] *Department of Chemistry, College of Science, King Saud University, PO BOX 2455, Riyadh 11451, Saudi Arabia*
[i] *Natural Products Research Laboratory, Strathclyde Institute of Pharmacy and Biomedical Sciences, University of Strathclyde, Glasgow G4 0RE, UK*
[j] *Division of Pathology, ICAR-Indian Veterinary Research Institute, Izatnagar, Bareilly 243122, Uttar Pradesh, India*

Received 27 July 2021; revised 30 September 2021; accepted 4 October 2021
Available online 19 October 2021

KEYWORDS

COVID-19;
DFT;
Molecular docking;
Molecular dynamics simulation;
Pharmacokinetic study;
QSAR

Abstract The current COVID-19 pandemic, caused by the severe acute respiratory syndrome coronavirus-2 (SARS-CoV-2) and its variants, remains a serious health hazard globally. The SARS-CoV-2 Mpro and spike proteins, as well as the human ACE2 receptor, have previously been reported as good targets for the development of new drug leads to combat COVID-19. Various ligands, including synthetic and plant-derived small molecules, can interact with the aforementioned proteins. In this study, we investigated the interaction of eight phytochemicals, from selected medicinal plants (*Aegle marmelos*, *Azadirachta indica*, and Ocimum sanctum) commonly used in Indian

* Corresponding authors.
E-mail addresses: ranjank_mohapatra@yahoo.com (R.K. Mohapatra), mahboobchem@gmail.com (M. Alam), mhashim@ksu.edu.sa (M. Azam), veronique.seidel@strath.ac.uk (
Veronique Seidel).
Peer review under responsibility of King Saud University.

Production and hosting by Elsevier

https://doi.org/10.1016/j.jscs.2021.101367

traditional medicine, with SARS-CoV-2 Mpro (PDBID: 6LU7), SARS-CoV-2S spike protein (PDB ID: 6M0J) and the human ACE2 receptor (PDB ID: 6M18). All compounds were subjected to density functional theory (DFT) and frontier molecular orbitals (FMO) analysis to determine their geometry, and key electronic and energetic properties. Upon examining the interactions of the phytochemicals with the human ACE2 receptor and the SARS-CoV-2 Mpro, spike protein targets, two compounds (C-5 and C-8) were identified as the best binding ligands. These were further examined in MD simulation studies to determine the stability of the ligand–protein interactions. QSAR, pharmacokinetic and drug-likeness properties studies revealed that C-5 may be the best candidate to serve as a template for the design and development of new drugs to combat COVID-19.

1. Introduction

The on-going COVID-19 pandemic, caused by the SARS-CoV-2 virus, remains a serious global health issue due to the highly contagious nature of this virus [1,2]. Unfortunately, the pandemic continues to have detrimental effects on all sectors of society [3]. The symptoms and clinical presentations of COVID-19 are complex, due in part to the ability of the virus to present rapid mutations in its spike protein receptor binding domain (RBD). The common symptoms include a dry cough, fever, shortness of breath, fatigue and dyspnoea. SARS-CoV-2 mainly transmits through respiratory aerosols/droplets from infected persons' coughs, sneezes, talks, breaths and via airborne transmission [2,4]. Other means of transmission such as direct and indirect contacts (e.g. via the fecal-oral route) have also been reported [5,6]. The virus infects the upper and lower respiratory tract, heart, kidney, liver, gut, nervous system and ultimately can lead to multi-organ damage [7]. Severe complications are frequently observed in immunocompromised individuals with diabetes, obesity, cardiovascular disorders and hypertension [8-10]. Different SARS-CoV-2 variants have been reported worldwide, with double and triple mutants of this virus present in some countries. These variants are highly transmissible (i.e. high infectivity and transmission rate), can cause re-infections, and there is some concern as to whether current vaccines can control all of them [11,12].

The main research efforts towards the discovery of new drugs to combat COVID-19 using computer-aided methodologies to date have focused on targeting the active site of SARS-CoV-2 Mpro and spike protein with small molecule ligands [13-15]. This has included studies on synthetic derivatives [16], including one study which identified six benzimidazole and benzothiazole derivatives with high binding affinity for SARS-CoV-2 (Mpro) and the human ACE2 receptor [12]. This has also included investigating phytochemicals to find potential inhibitors of Mpro through virtual screening and structure-based drug discovery approaches [17-19]. For example, Lakshmi and co-workers [20] investigated 47 phytochemicals against SARS-CoV-2 (Mpro), SARS-CoV-2S and the human ACE2 receptor. Another study investigated 27 caffeic-acid derivatives against several proteins of SARS-CoV-2, reporting MD simulations, ADME properties and toxicity profiles of these derivatives [21].

In this study, we report on the binding affinity of eight phytochemicals from three medicinal plants against SARS CoV-2 (Mpro and spike protein) and the human ACE2 receptor using an *in silico* docking approach. The selected phytochemicals include 3′-prenyloxypsoralen (1), imperatorin (2), and xanthotoxin (3) from *A. marmelos*; epicatechin (4), margolonone (5) and gedunin (6) from *A. indica*; chlorogenic acid (7) and luteolin-7-*O*-glucuronide (8) from *Ocimum* spp. (Fig. 1). Molecular dynamics simulation studies were further performed to determine the stability of selected phytochemical-protein interactions. We also report on DFT (density functional theory) calculations, pharmacokinetic and drug-likeness predictions.

2. Materials and methods

2.1. Computational studies (DFT)

The selected phytochemicals were first optimized using the Gauss View 6.0.16 program [22] and subjected to density functional theory (DFT) calculation using the GAUSSIAN 09 suite programs [23]. Computations were executed using the B3LYP method and exchange–correlation functional with 6-31 G (d, p) basic set for the calculation of carbon, nitrogen, oxygen, sulphur and hydrogen atoms.

2.2. Molecular docking study

The binding affinities of ligands can be predicted using molecular docking protocols [24]. Receptor-oriented flexible docking was carried out using the Autodock Vina package. The selected phytochemicals were docked against three essential targets, namely SARS-CoV-2 Mpro (PDB ID: 6LU7), ACE2 (PDB ID:6M18) and SARS-CoV-2S spike protein (PDB ID: 6M0J). The three-dimensional crystal structure of SARS-CoV-2 Mpro (PDB ID: 6LU7), SARS-CoV-2S (PDB ID: 6M0J) and the human ACE2 receptor (PDB ID: 6M18) were retrieved from the Protein Data Bank (http://www.rcsb.org/pdb). Prior to the docking process, all ligands and the proteins were prepared and saved as pdbqt files. The Autodock Tools software was used to attribute polar hydrogens, solvation parameters, Kollman charges and fragmental volumes to each protein. It was also used to create a grid box around the binding site of each protein. The configuration file for the grid parameters was generated using the Auto grid engine. During the docking procedure, the ligands and proteins were considered as flexible. Results < 1.0 Å in positional RMSD clustered together and represented the best binding free energy. The best pose with the lowest docking score (binding energy or binding affinity) was used for further analysis. Discovery Studio 3.5

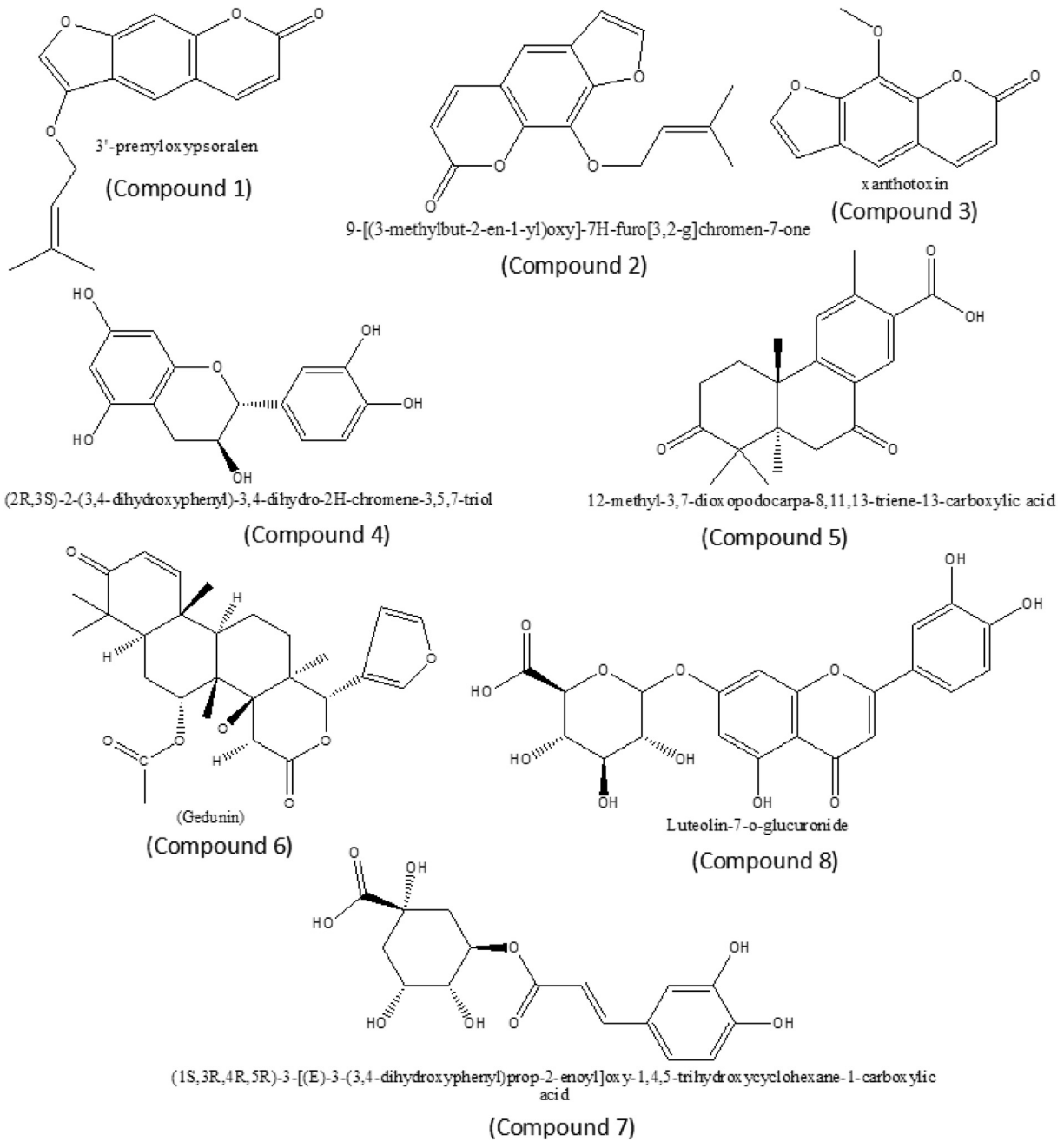

Fig. 1 Structure of the investigated plant-based compounds C1-C8.

was used to visualize the 2-D and 3-D interactions between ligand atoms and protein amino acid residues.

2.3. Molecular dynamics simulation

MD simulations were carried out to evaluate the stability of the protein–ligand complex. This was carried out only for the best complexes (C8-6LU7, C5-6M18, and C8-6M0J) using the Desmond MD simulation package of Schrodinger [25]. The OPLS_2005 force field was used for the protein–ligand complexes. These complexes were solvated in a cubical water box (TIP3P water model) in x, y and z dimensions using the system builder tool of Desmond keeping 12 Å buffer space. As and when required, each system was neutralized by the addition of suitable counter ions. The neutralization was maintained by adding an ionic concentration of 0.15 M NaCl. 10,000 steepest descent steps were used to minimize the systems followed by gradual heating from 0 to 300 K, under NVT ensemble. Before each run, the systems were allowed to relax thermally using the Nose-Hoover Chain thermostat method for 5 ns and pressure relaxation for 5 ns using the Martyna-Tobias-Klein barostat method. A 100 ns run was performed under the NPT ensemble using a cut-off distance of 12 Å. Trajectories of 5000 frames were generated and saved at every 10 ps.

2.4. Pharmacokinetic and drug-likeness predictions

The SwissADME online software was used to predict the pharmacokinetic properties of the investigated compounds. This included their drug-likeness properties, solubility and other properties. The Lipinski's properties were determined using the PubChem database. A work flow diagram of the methodology used is illustrated in Scheme 1.

3. Results and discussion

3.1. Molecular modelling studies

Density Functional Theory (DFT) calculations, using the commonly-employed GAUSSIAN inter phase, were used to theoretically outline the structural projections and atomic arrangements of the studied compounds. The use of exchange–correlation functional enabled to estimate molecular properties with precision comparable to conventional correlated *ab-initio* methods [26,27]. Molecular orbitals (MOs) geometry optimization studies were used to evaluate the geometry and electronic properties of compounds [28-33]. The key energetic properties such as single point energy and dipole moment (D) values for each compounds are presented in Table 1. It was observed that compound C-3 had a considerably higher single point energy than all other compounds. Compound C-8 showed the least energy among all compounds, which indicated a greater stability. All compounds possessed dipole–dipole interactions, but compound C-2 had a higher dipole moment value compared to others.

Table 1 Molecular formulas and estimated energetic properties of the compounds.

Compounds	Molecular formula	Single point energy (kcal/mol)	Dipole moment (D)
(C-1)	$C_{16}H_{14}O_4$	-5.7664×10^5	0.696
(C-2)	$C_{16}H_{14}O_4$	-5.7609×10^5	2.739
(C-3)	$C_{12}H_8O_4$	-4.7871×10^5	−0.312
(C-4)	$C_{15}H_{14}O_6$	-6.4719×10^5	1.175
(C-5)	$C_{20}H_{24}O_4$	-6.7609×10^5	0.820
(C-6)	$C_{28}H_{36}O_7$	-10.1325×10^5	0.674
(C-7)	$C_{16}H_{18}O_9$	-8.8412×10^5	0.956
(C-8)	$C_{21}H_{18}O_{12}$	-10.7509×10^5	0.082

3.2. FMOs approach

FMOs studies are helpful to understand the reactivity of compounds and identify the reactive site in conjugated systems.

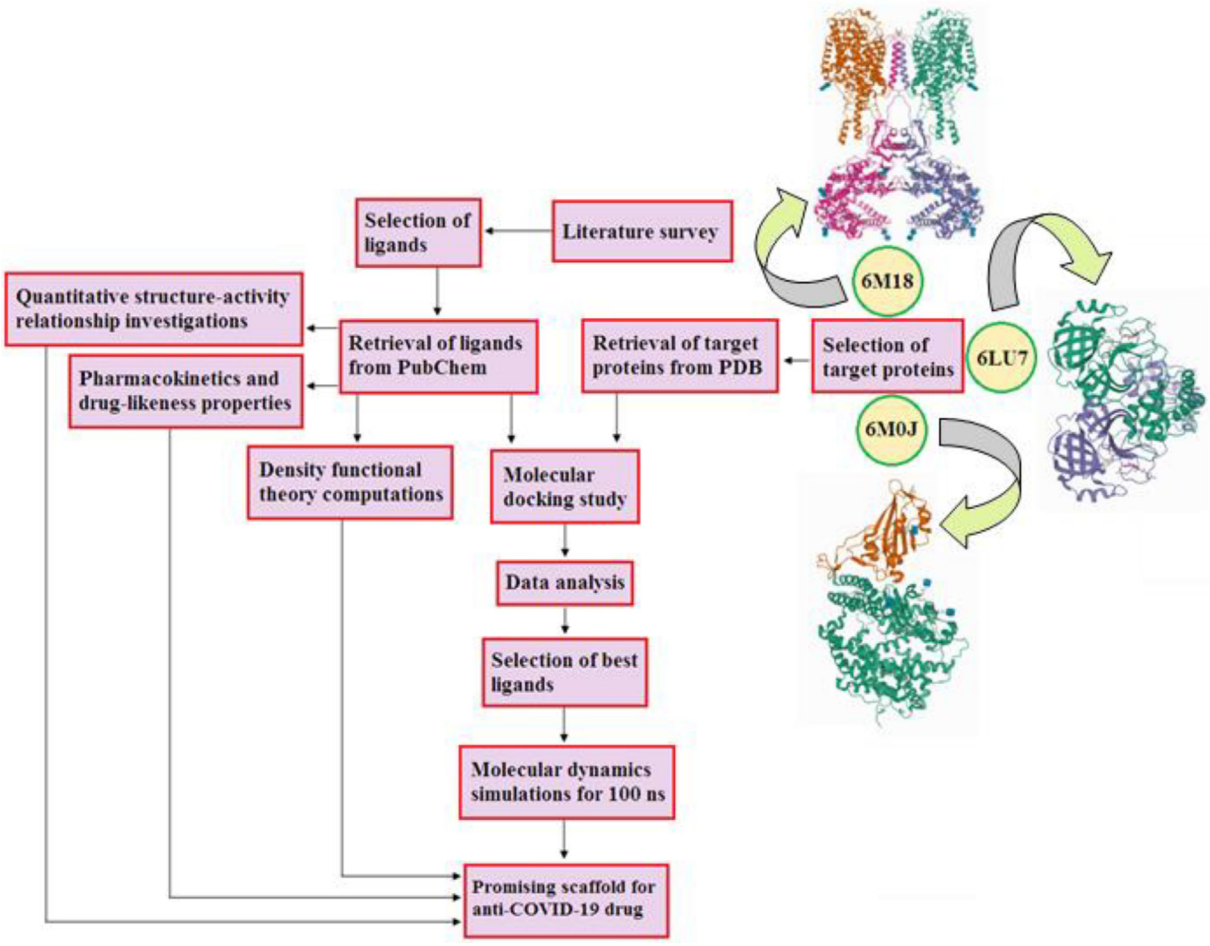

Scheme 1 Work flow diagram of the methodology used in the study.

Table 2 Computed quantum chemical parameters for the compounds.

Compound	HOMO (eV)	LUMO (eV)	ΔE (eV)	χ Pauling	η (eV)	σ	μ (eV)	S	ω (ev)
C-1	−0.2476	−0.0705	0.1771	−0.1590	0.0885	11.29	0.1590	5.649	0.141
C-2	−0.1381	−0.0713	0.0668	−0.1015	0.0334	29.94	0.1015	14.97	0.154
C-3	−0.2368	−0.0833	0.1535	−0.1600	0.0767	13.03	0.1600	6.518	0.166
C-4	−0.2353	−0.0362	0.1991	−0.1357	0.0995	10.05	0.1357	5.025	0.092
C-5	−0.2550	−0.0726	0.1824	−0.1638	0.0912	10.96	0.1638	5.464	0.227
C-6	−0.2433	−0.0603	0.183	−0.1518	0.0915	10.92	0.1518	5.462	0.125
C-7	−0.1939	−0.0768	0.1171	−0.1353	0.0585	17.09	0.1353	8.547	0.156
C-8	−0.1996	−0.0810	0.1186	−0.1403	0.0593	16.86	0.1403	8.474	0.164

Table 3 QSAR data for the compounds.

Function	C-1	C-2	C-3	C-4	C-5	C-6	C-7	C-8
Surface area (Approx) ($Å^2$)	449.97	305.66	297.84	375.72	449.86	514.50	452.91	883.31
Surface area (Grid) ($Å^2$)	449.68	432.12	389.82	478.86	502.45	626.74	560.76	639.81
Volume ($Å^3$)	810.13	720.89	608.34	787.86	877.82	118.40	920.49	1092.10
Hydration energy (kcal/mol)	−9.63	−5.76	−8.94	−32.62	−7.66	−9.03	−33.30	−41.62
Log P	4.75	4.75	3.21	2.18	9.30	9.14	3.93	4.93
Refractivity ($Å^3$)	27.82	27.82	16.91	29.31	59.38	96.30	46.73	47.68
Polarizability ($Å^3$)	28.66	28.66	21.51	28.65	35.47	50.51	32.45	41.41
Mass (amu)	270.80	270.28	216.19	290.27	328.41	484.59	354.31	462.37
Total energy (kcal/mol)	151.035	770.922	93.384	70.477	288.24	823.34	170.06	496.12
Dipole Moment (Debye)	0.44	0.44	0.44	3.267	1.11	0.808	2.22	3.94
Free energy (kcal/mol)	151.035	770.922	93.384	70.477	288.24	823.34	170.06	496.12
RMS Gradient (kcal/Å mol)	68.34	116.6	51.05	33.9	68.19	92.69	55.6	98.01

The computed E_{HOMO} and E_{LUMO} of all compounds clearly explained the global reactivity descriptors. The negative values for E_{HOMO} and E_{LUMO} for all investigated compounds indicate their stability [34]. The energy gap (band gap) corresponds to the chemical reactivity and chemical stability behaviour of active molecules [35]. C-2 was found to have the least energy difference [E_{HOMO} - E_{LUMO}] among all compounds. The energy difference values obtained suggest that the reactivity of C-3 will be the greatest, and the stability of C-4, C-5, C-7 and C-8 will be greatest among all compounds. The E_{HOMO} and E_{LUMO} variation describes the charge transfer (CT) fundamental interaction. To get some conclusive evidence, a range of chemical reactivity parameters such as chemical potential (μ), electronegativity (χ), global softness (S), global hardness (η), and global electrophilicity index (ω) [36] were calculated (Table 2).

The chemical softness (S) values obtained for C-1, C-3, C-4, C-5, C-6 were less compared to C-7, C-8 (moderate) and C-2 (maximum), which explains the compounds stability. A compound is more reactive if it has a high chemical softness value and in reverse, for smaller values, reactivity decreases and stability increases [30,32]. The electrophilicity (ω) value is another important parameter, and positive values measures the flow of the system to gain electron from the surrounding [30,32]. We observed that C-4 was the most stable compound because it had a low electrophilicity value compared to other compounds (Table 2).

3.3. QSAR studies

QSAR studies were used to anticipate the reactivity and properties of the selected compounds. The computational calculation was carried out using the HyperChem Professional 8.0.3 program. Initially, all compounds were optimized using the (MM^+) force field, with semi-empirical PM3 methods, and energy minimization was achieved using a Fletcher-Reeves conjugate gradient algorithm method. We found that the partition coefficient (log P) value for C-5 was greater than the rest of the compounds. Log P values are important to evaluate the biological activity of compounds and estimate their permeability into cell membranes [37]. Other key parameters such as Refractivity, Polarizability, Mass, Volume, Hydration energy, Surface area, Total energy, Free energy and RMS Gradient were also estimated for all compounds (Table 3).

3.4. Molecular docking study

Molecular docking was used to predict the binding interactions between each protein and the selected phytochemicals (ligands). The three-dimensional crystal structure of SARS-CoV-2 Mpro (PDB ID: 6LU7), SARS-CoV-2S (PDB ID: 6M0J) and the human ACE2 receptor (PDB ID: 6M18) were used as the biological targets for the docking analysis. We investigated eight previously reported phytochemicals from different natural sources [38-40]. All phytochemicals interacted with the main protease (Mpro) by docking in the binding pocket cavity comprising of common amino acid residues including ARG131, LYS137, THR199, TYR239 and LEU287. The best docking (binding free energy) scores for all phytochemicals were found in the range −6.2 to −7.9. Compound C-2 exhibited a binding energy value of −6.2 while C-8 had a binding energy value of −7.9. Detailed interactions are depicted in Fig. 2 and Table-S1. These ligands were also

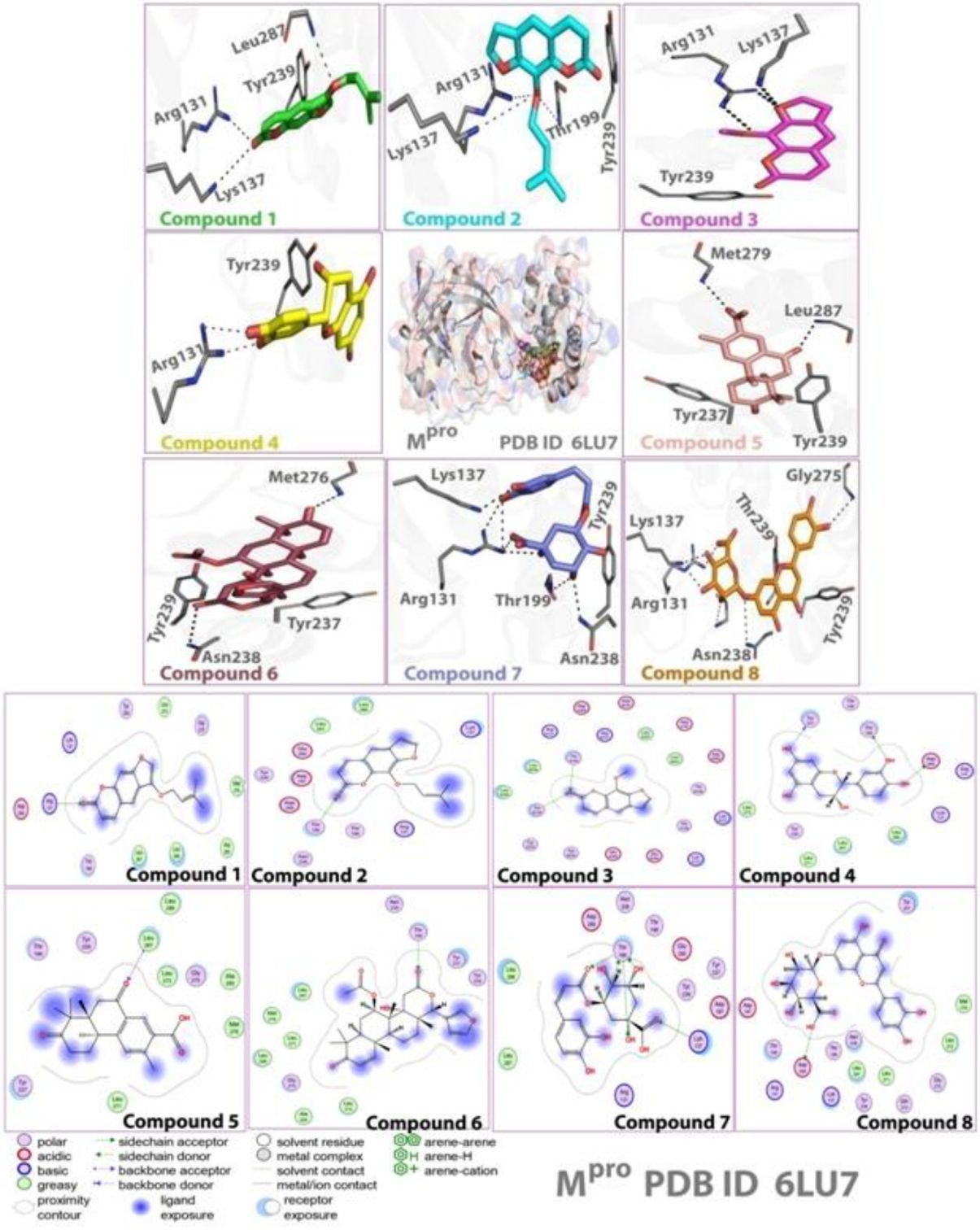

Fig. 2 Ligand-receptor interactions of compounds (C1-C8) with SARS-CoV-2 (Mpro).

docked with the human ACE2 RBD. Compound C-3 showed a binding affinity for ACE2 with a docking score of −6.3, whereas compounds C-5, C-6 and C-8 were predicted to have higher binding energies (Fig. 3 and Table-S2). The docking scores obtained for each compound interacting with the SARS-CoV-2 spike protein receptor are presented in Fig. 4 and Table-S3. Binding energy values for all compounds ranged from −6.4 to −7.6, with C-5, C-6, C-7 and C-8 exhibiting the highest binding energy values.

Taking all targets into consideration, we found that C-5, C-6 and C-8 exhibited the highest binding affinity values. Based on their scoring values, these compounds were further inspected

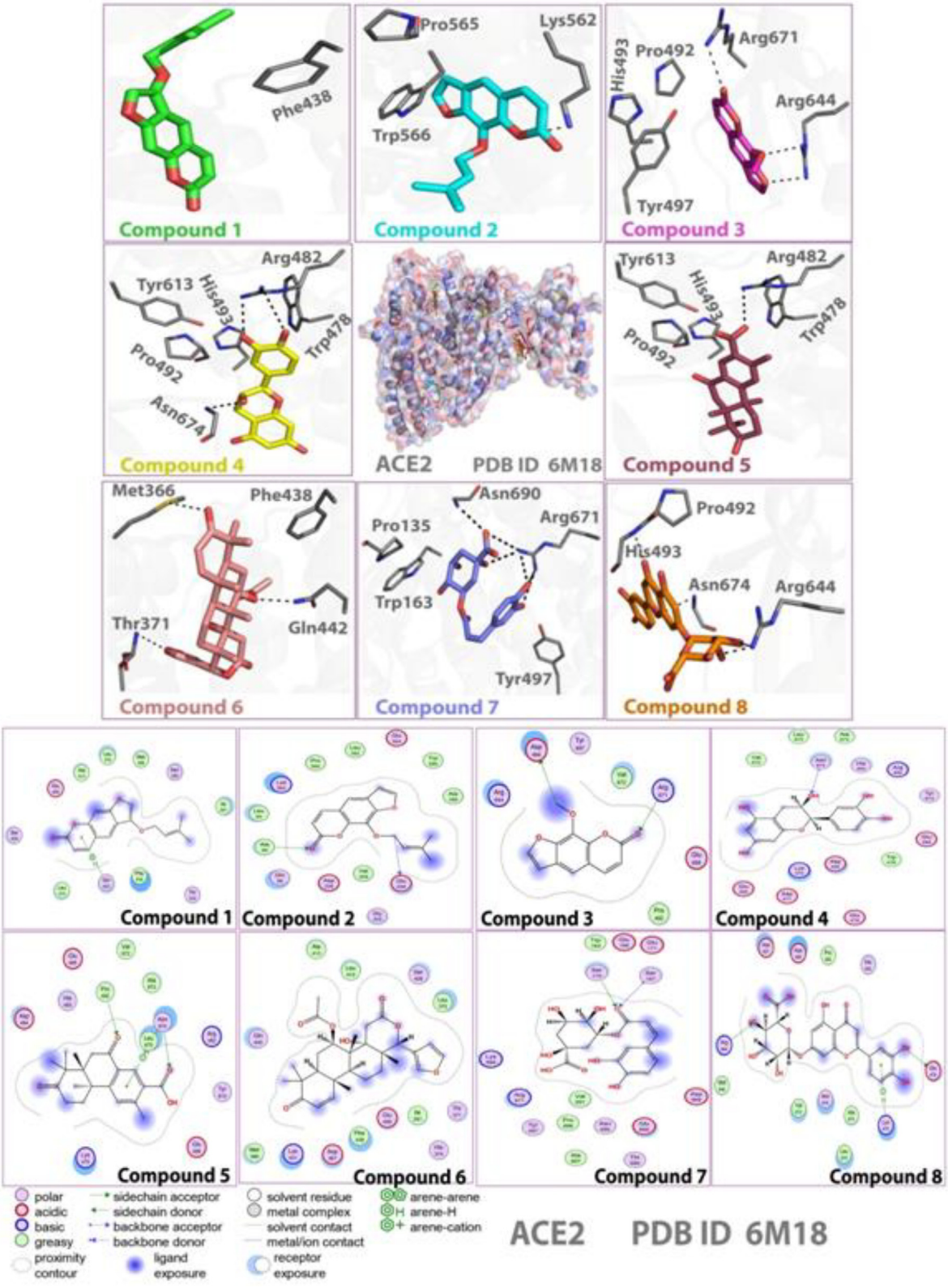

Fig. 3 Ligand-receptor interactions of compounds (C1-C8) with ACE2.

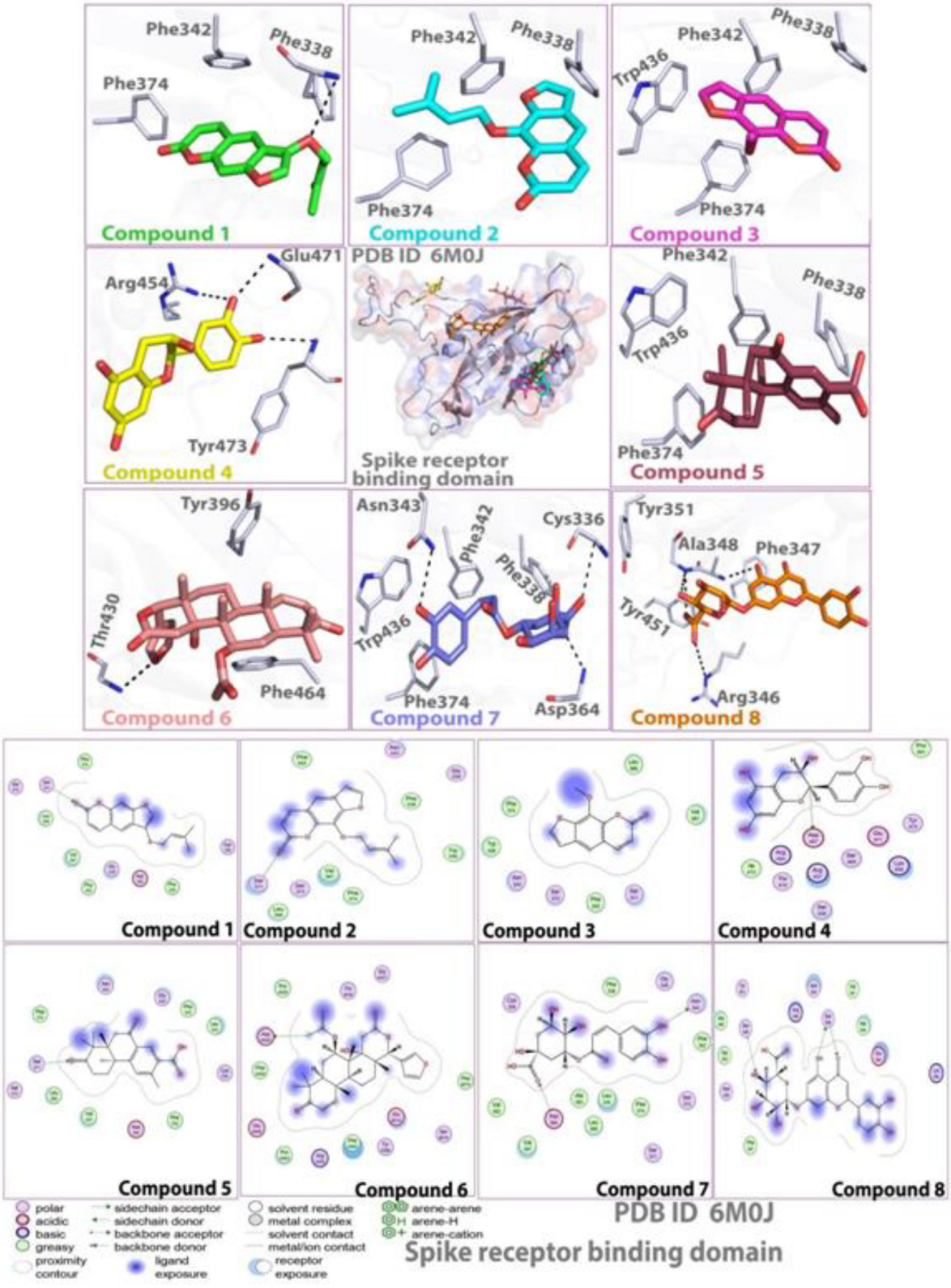

Fig. 4 Ligand-receptor interactions of compounds (C1-C8) with SARS-CoV-2S.

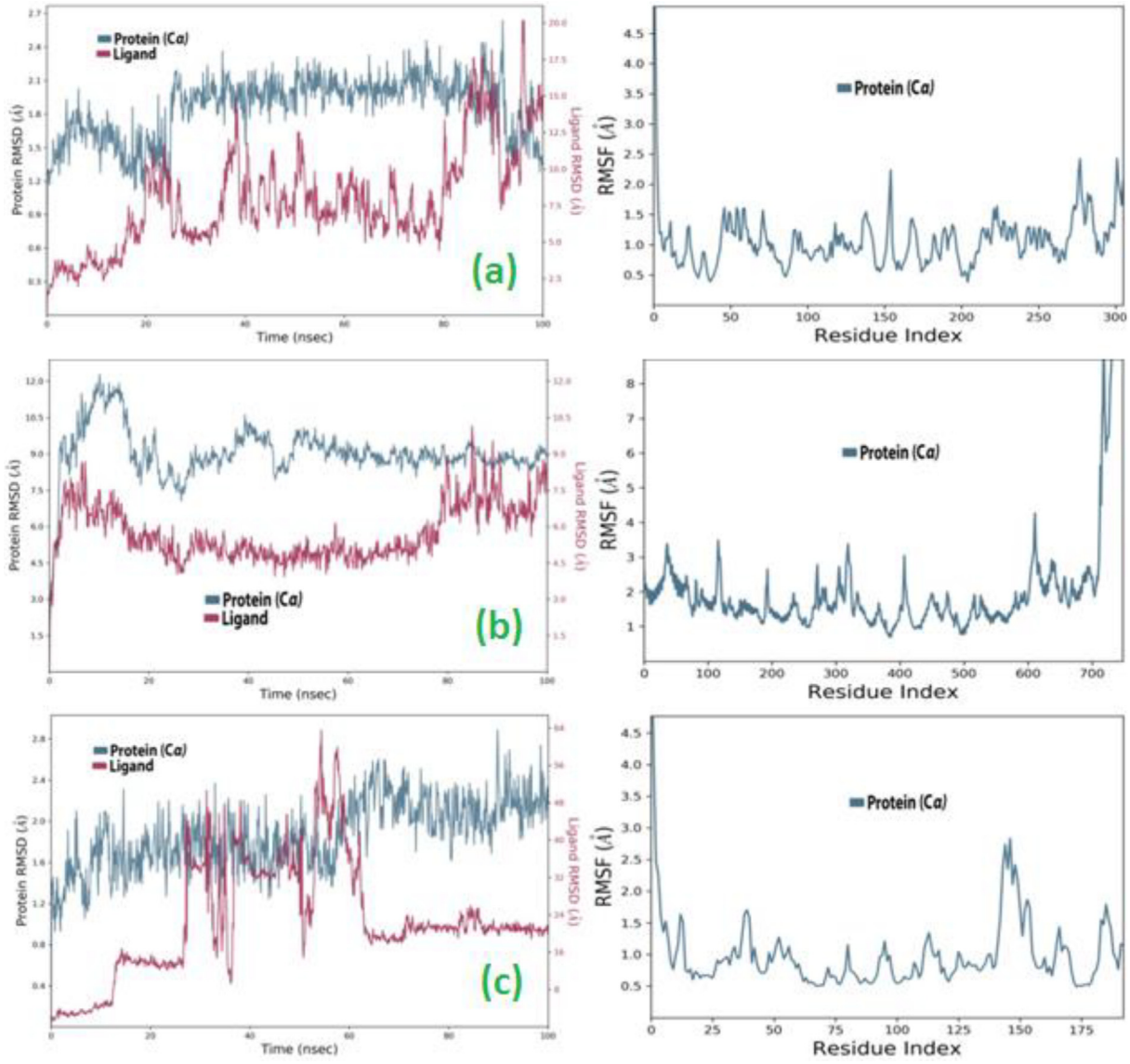

Fig. 5 Protein RMSD and RMSF trajectory of (a) (C8-6LU7) complex, (b) (C5-6M18) complex, (c) (C8-6M0J) complex.

for their interactions with the targets, in terms of hydrophobic, hydrogens and other bonding types. Almost all compounds showed interactions with key amino acid residues of Mpro (THR 199, ASP 289, LYS 137, ARG 131, LEU 287, TYR 237), the ACE2 receptor (GLN 442, GLU 208, GLU 479, ASP 494, ARG 671, ARG 644, ASN 674, SER 167, SER 170, LYS 475) and SARS CoV-2S (SER 371, SER 399, SER 349, ASP 467, ASP 428, ASP 364, ASN 343) [12,15,16,19].

3.5. Molecular dynamics simulation

As margolonone (C-5) from *A. indica*, and luteolin-7-*O*-glucuronide (C-8) from *Ocimum* spp. revealed significant interactions with the protein targets in the molecular docking study, these compounds were chosen as the best ligands for further MD simulation work. A molecular dynamics simulation of 100 ns was carried out for these compounds to get better insights into the stability of the protein–ligand complexes. The overall stability was further investigated through RMSD and RMSF analysis.

3.5.1. Protein RMSD

MD simulation was run as reported earlier to investigate the stability of each ligand–protein interactions [41]. MD simulations were performed for the best complex (C8-6LU7, C5-6M18, and C8-6M0J) [15,42]. The ligand–protein complexes were simulated for 100 ns to analyze RMSD and RMSF (Fig. 5). For the C8-6LU7 complex, the protein achieved a maximum RMSD (2.6 Å) at 90 ns and then gradually came to an equilibrium reaching 1.3 Å. The ligand showed initial fluctuations, then reached 20.0 Å and became stable reaching 15.0 Å at 100 ns for the same complex (Fig. 5a). The RMSF

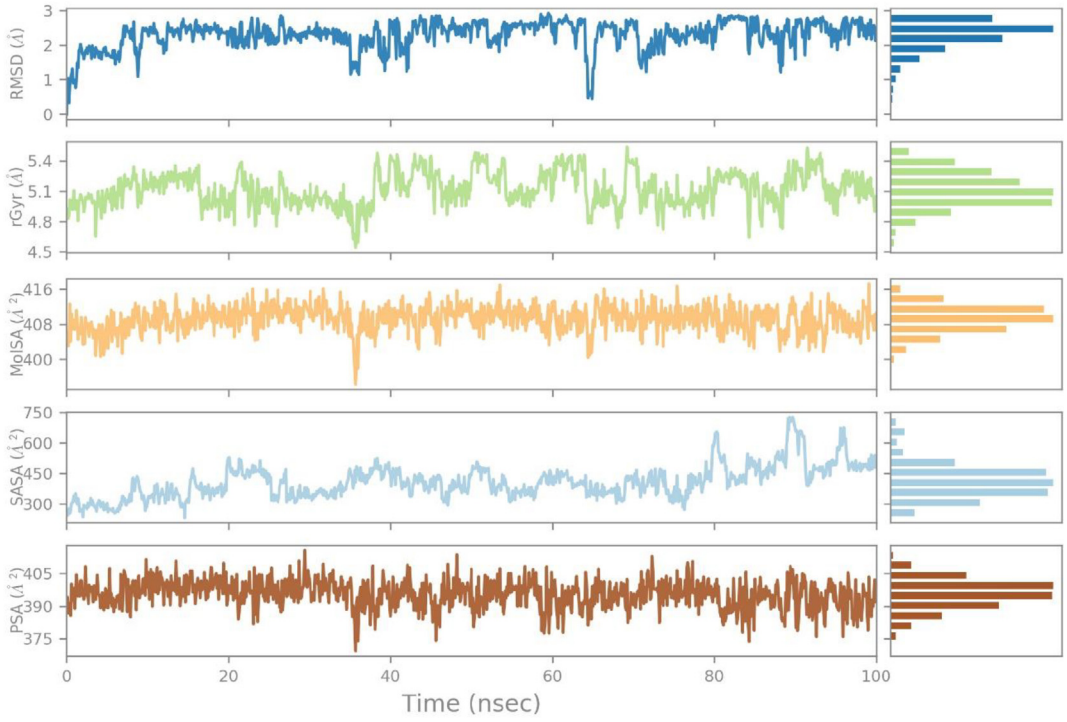

Fig. 6 Ligand property trajectory of the (C8-6LU7) complex.

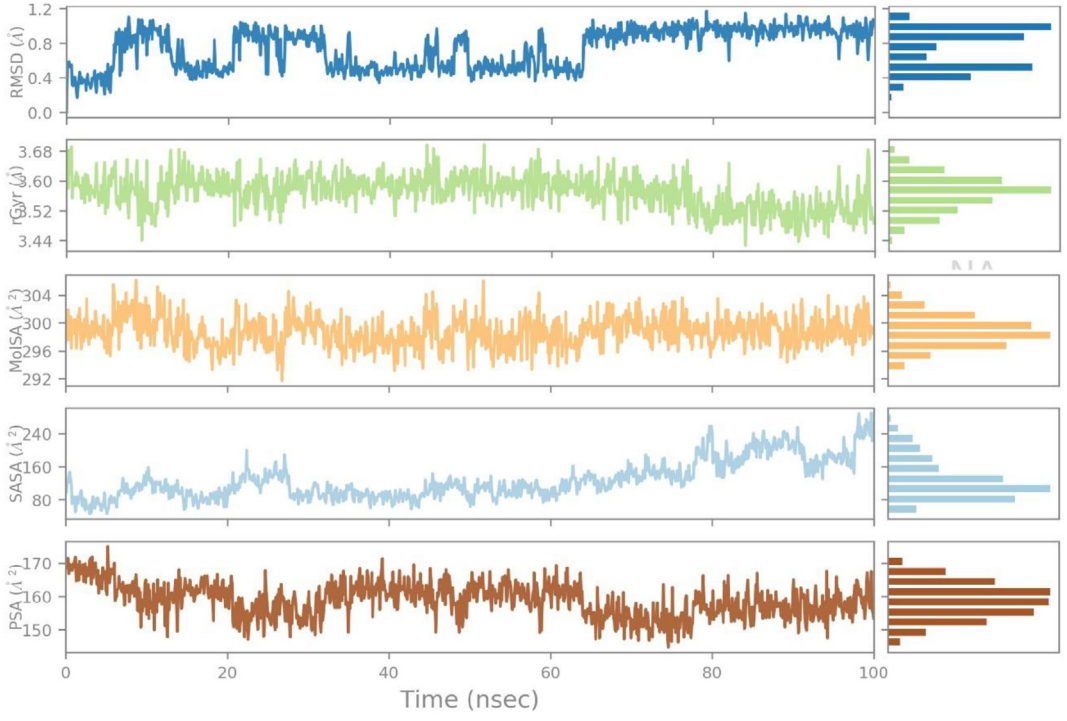

Fig. 7 Ligand property trajectory of the (C5-6M18) complex.

remained less than 2.5 Å throughout the simulation (Fig. 5a). The protein RMSD trajectory for the C5-6M18 complex achieved a maximum root means square deviation (12.0 Å) at 10 ns, decreased further up to 100 ns and then became stable at 9.0 Å. The ligand showed fluctuations initially and then gradually reached equilibrium (Fig. 5b). The RMSF was less than 4.5 Å for the complex (Fig. 5b). For the C8-6M0J complex, the protein achieved a maximum RMSD (2.8 Å) at

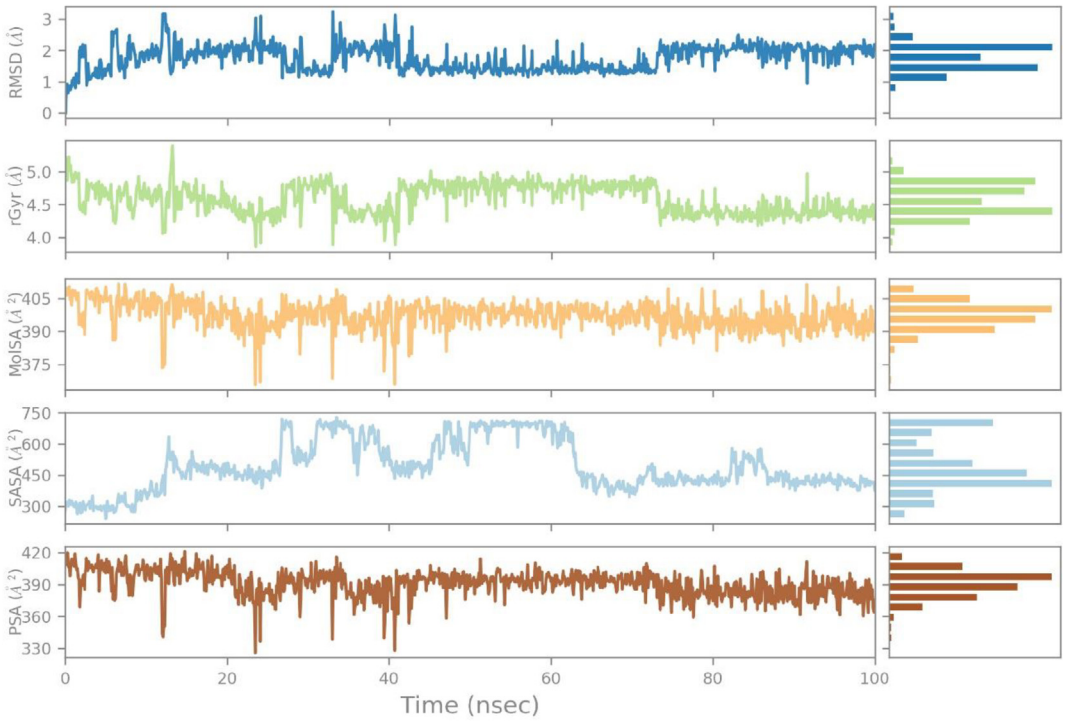

Fig. 8 Ligand property trajectory of the (C8-6M0J) complex.

90 ns and then gradually came to an equilibrium. The ligand showed fluctuations initially and reached 64.0 Å at 55 ns and became stable reaching 21.0 Å at 100 ns (Fig. 5c). The RMSF was less than 3.0 Å for the complex throughout the simulation (Fig. 5c). The RMSD average value of Mpro (6LU7), ACE2 (6M18) and the spike protein (6M0J) at equilibrium was found to be 2.1 Å, 9.0 Å and 1.6 Å, respectively. A deviation within 1–3 Å is acceptable for small globular proteins [15,41,42]. These complexes were further used for protein–ligand contact analysis.

3.5.2. Ligand properties

Ligand properties were analyzed by calculating Ligand RMSD, Molecular Surface Area (MolSA), Radius of Gyration (rGyr), Polar Surface Area (PSA) and Solvent Accessible Surface Area (SASA). The RMSD of ligands initially fluctuated up to 10 ns for C8-6LU7, C5-6M18 and C8-6M0J, then gradually reached an equilibrium. The ligands RMSD values ranged from around 0.5 to 3.0 Å with equilibrium at 2.2 Å (C8-6LU7), around 0.2 to 1.2 Å and equilibrium at 1.1 Å (C5-6M18), and around 0.8 to 3.0 Å and equilibrium at 2.0 Å (C8-6M0J) (Figs. 6-8). The rGyr of the ligands showed slight fluctuation and then gradually reached an equilibrium. The ligands displayed rGyr values ranging from around 4.5 to 5.5 Å and equilibrium at 5.0 Å (C8-6LU7), around 3.44 to 3.68 Å and equilibrium at 3.52 Å (C5-6M18), and around 4.0 to 5.5 Å and equilibrium at 4.3 Å (C8-6M0J) (Figs. 6–8).

The ligands showed MolSA values ranging from around 396 to 416 $Å^2$ with equilibrium at 408 $Å^2$ (C8-6LU7), around 292 to 304 $Å^2$ with equilibrium around 298 $Å^2$ (C5-6M18), and around 370 to 410 Å with equilibrium at 395 Å (C8-6M0J) (Figs. 6-8). The SASA values of the ligands started with a slight fluctuation and then gradually reached equilibrium. The ligands displayed a SASA values ranging from around 300 to 750 $Å^2$ with equilibrium at 470 $Å^2$ (C8-6LU7), around 50 to 280 $Å^2$ with equilibrium at 240 $Å^2$ (C5-6M18), and around 300 to 750 $Å^2$ with equilibrium at 420 $Å^2$ (C8-6M0J). The solvent accessible surface area (PSA) was nearly constant throughout the simulation. The ligands showed PSA values ranging from around 375 to 405 $Å^2$ with equilibrium at 390 $Å^2$ (C8-6LU7), around 145 to 175 $Å^2$ with equilibrium at 160 $Å^2$ (C5-6M18), and around 330 to 420 $Å^2$ with equilibrium at 360 $Å^2$ (C8-6M0J). The ligand properties showed minimum fluctuation in the initial stage of the simulation, gradually reached an equilibrium and then remained constant throughout the simulation. This confirmed that the ligands were stable in the active site of the proteins.

3.5.3. Protein-ligand contacts

The protein-ligand (P-L) contacts for these stable complexes were studied using contact histograms (Figs. 9–11) [43]. The P-L interactions were classified into four types, including hydrophobic, ionic, hydrogen bonds, and water bridges. Hydrogen bonds play a crucial role in ligand binding and, as such, are crucial to take into account in drug design. The histograms displaying active site amino acids (mainly LYS-137, ASP-197, THR-199, LEU-272, MET-276, ALA-285, LEU-287, ASP-289 for 6LU7; LYS-475, GLU-489, TYR-613, VAL-672, ASN-674, LEU-675 for 6M18; and GLU-340, VAL-341, ASN-343, ALA-344, THR-345, ARG-346, ALA-348, GLY-381, SER-399, TYR-449, ASN-450, GLU-484 for 6M0J) interacting through hydrogen bonds with the ligands are shown in Figs. 9-11. The amino acids (mainly TYR-237, LEU-286, ALA-285, LEU-287 for 6LU7; TRP-478,

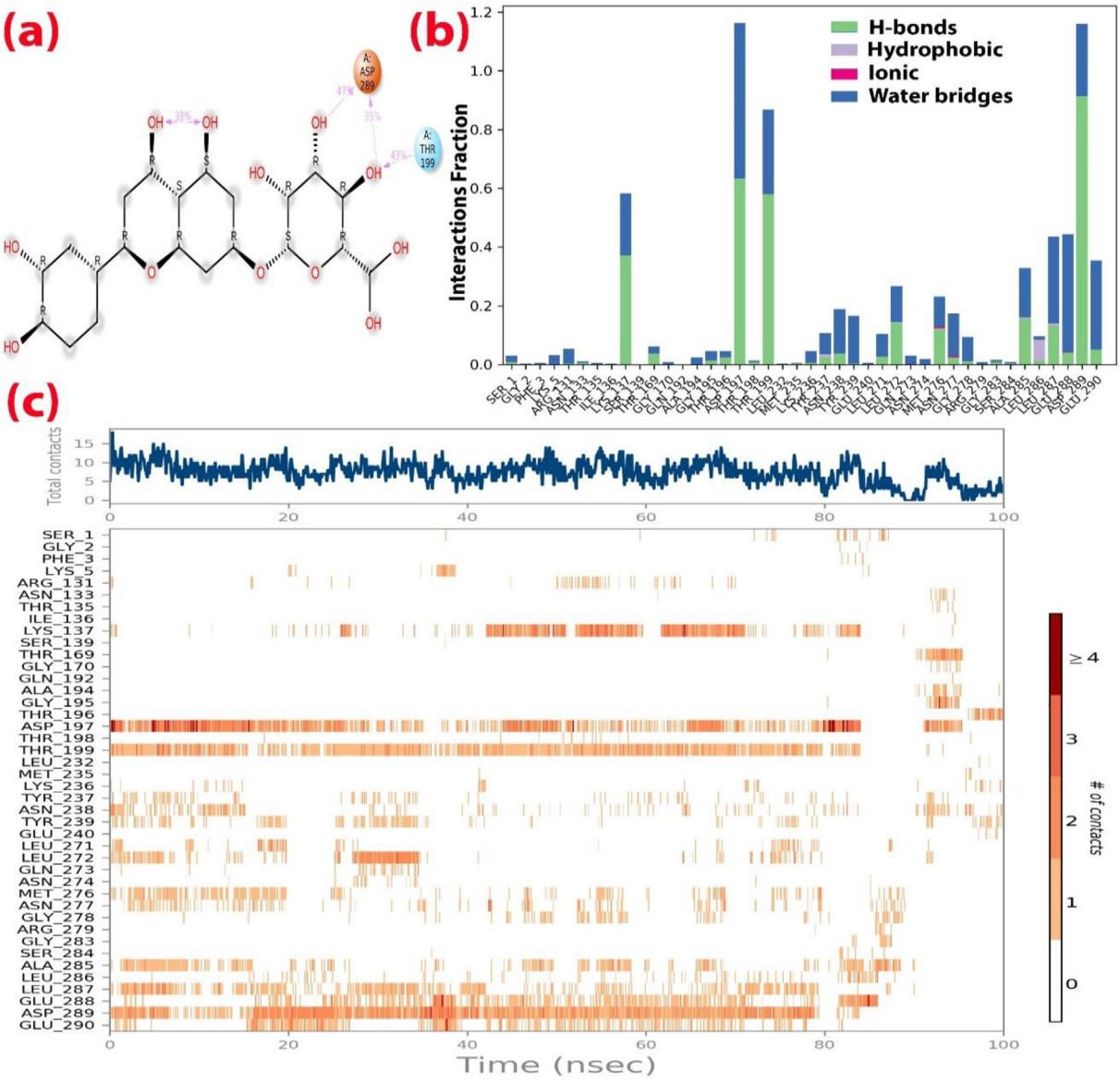

Fig. 9 Protein-ligand contact plots and interaction residues for the (C8-6LU7) complex.

PRO-492, MET-640, VAL-672, LEU-675 for 6M18; and ALA-344, TYR-449, LEU-452, PHE-490 for 6M0J) involved in hydrophobic interactions are also shown in Figs. 8-10. Residues MET-276, ASN-277 for 6LU7 and LYS-475 for 6M18 and ARG-346, LYS-356, LYS-444 for 6M0J showed some ionic interactions with the ligands. Residues ARG-131, LYS-137, ASP-197, THR-199, TYR-239, ALA-285, LEU-287, GLU-288, ASP-289, GLU-290 for 6LU7; ASP-471, LYS-475, GLU-479, ARG-482, ASP-494, GLU-495, TYR-613, ASP-637, ARG-644, VAL-672, ASN-674, LEU-675 for 6M18; and GLU-340, ASN-343, THR-345, ARG-346, ASN-354, LYS-356, GLY-446, TYR-449, ASN-450, TYR-451, THR-470, SER-494, TYR-495 for 6M0J interacted with the ligands via water bridges. The number of contact varied between 0 and 15 for 6LU7, 0 to 9 for 6M18 and 0 to 12 for 6M0J over the course of the trajectory. The contribution of amino acids was analyzed from the P-L interaction in each trajectory frame. The receptor-ligand complex showed deep bands (ASP-197, THR-199, ASP-289 for C8-6LU7; GLU-489, ASN-674, LEU-675 for C5-6M18; and TYR-449 for C8-6M0J), which indicated that the above amino acid residues had more interactions with the ligands in all possible orientations.

3.6. Pharmacokinetics and drug-likeness predictions

The pharmacokinetic and drug-likeness properties of the investigated compounds were calculated (Fig. 12 and Tables S4-S9). *In-silico* pharmacokinetic studies are used as an effective approach towards the search and design of potential small drug-leads for a specific target [44]. All compounds (except for C-4, C-6, C-7, C-8) obeyed the Lipinski's Rule of Five

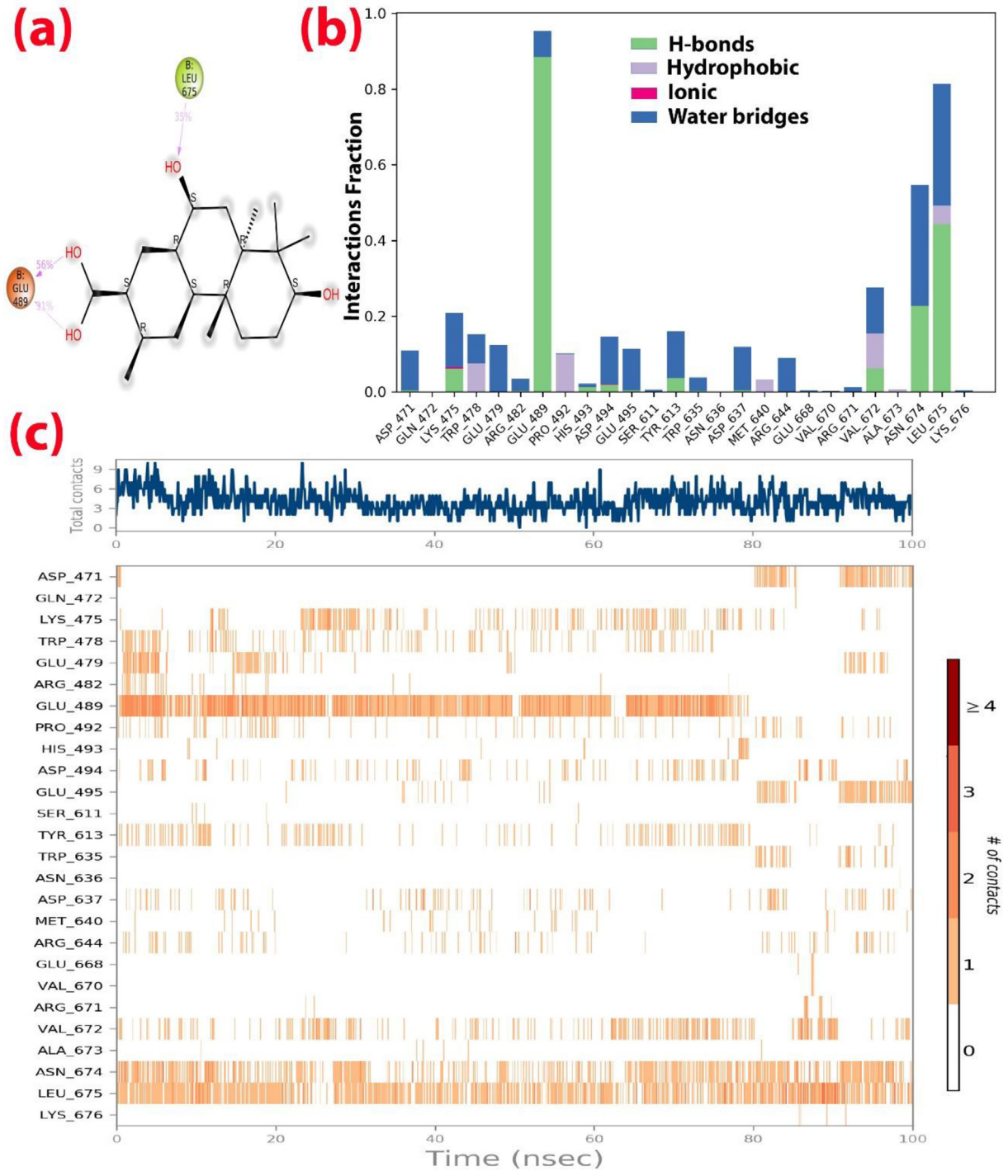

Fig. 10 Protein-ligand contact plots and interaction residues for the **(**C5-6M18**)** complex.

(Ro5), with a molecular weight < 500 g/mol, number of hydrogen bond donors and acceptors < 5, logP value < 5 and molar refractivity < 140 [45,46]. The TPSA of all compounds (except for C-7, C-8) was less than 110 $Å^2$, indicating the potentiality of these compounds as favourable drug molecules [43]. The number of rotatable bonds for all compounds was ≤5, suggesting that these compounds are flexible in nature. In addition, all compounds (except for C-7, C-8) were soluble and highly absorbable in the gastrointestinal tract. The synthetic accessibility value of the compounds was ≤6, which indicated their feasibility of synthesis. Drug-likeness filters such as, Ghose, Egan, Veber, and Muegge filters were also used to enhance the predictions. As C-6, C-7, C-8 did not obey the rules for oral drug-likeness, these compounds may be administered through other routes. Our results indicate that C5, however, is the best candidate for oral administration.

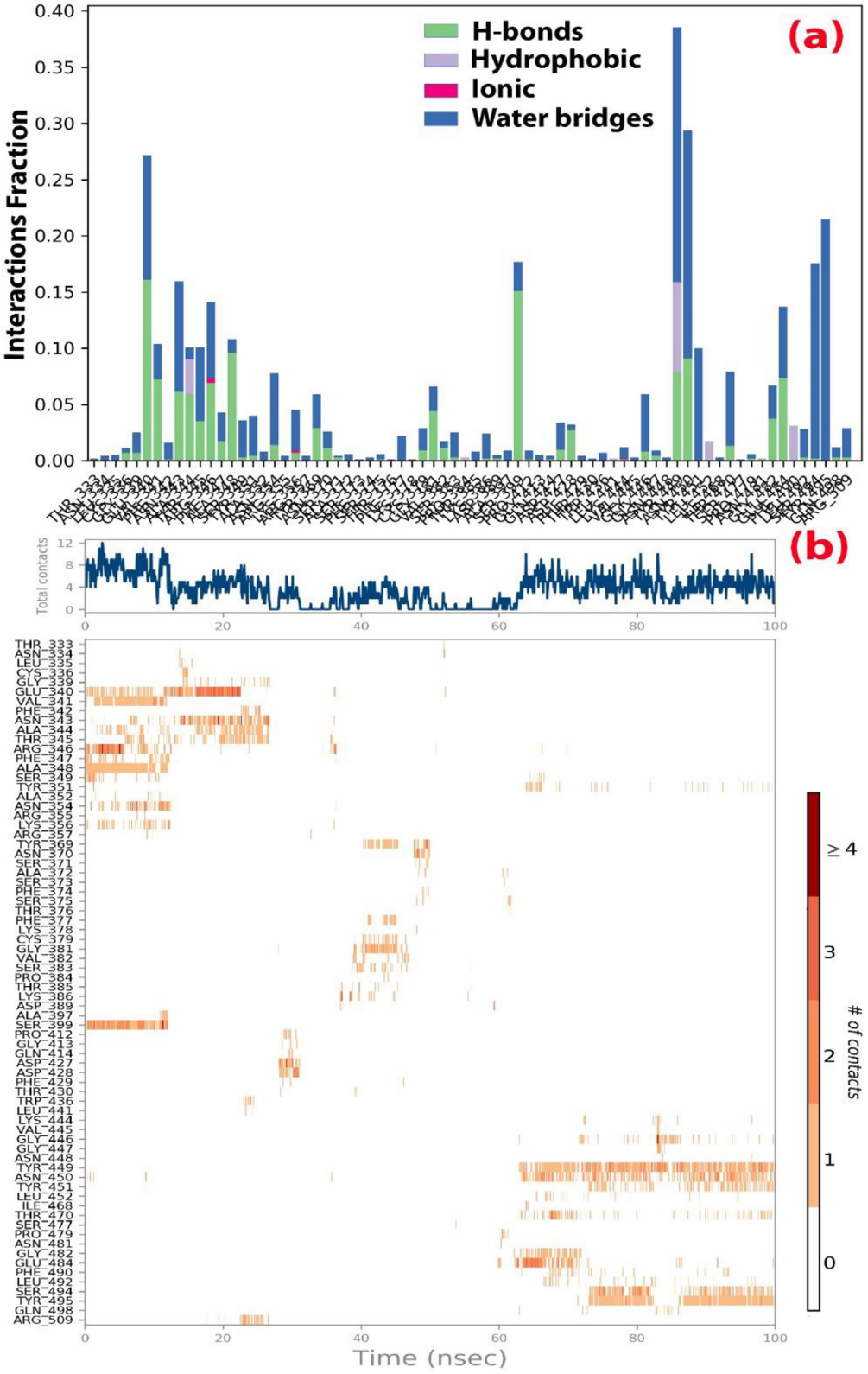

Fig. 11 Protein-ligand contact plots and interaction residues for the **(**C8-6M0J**)** complex.

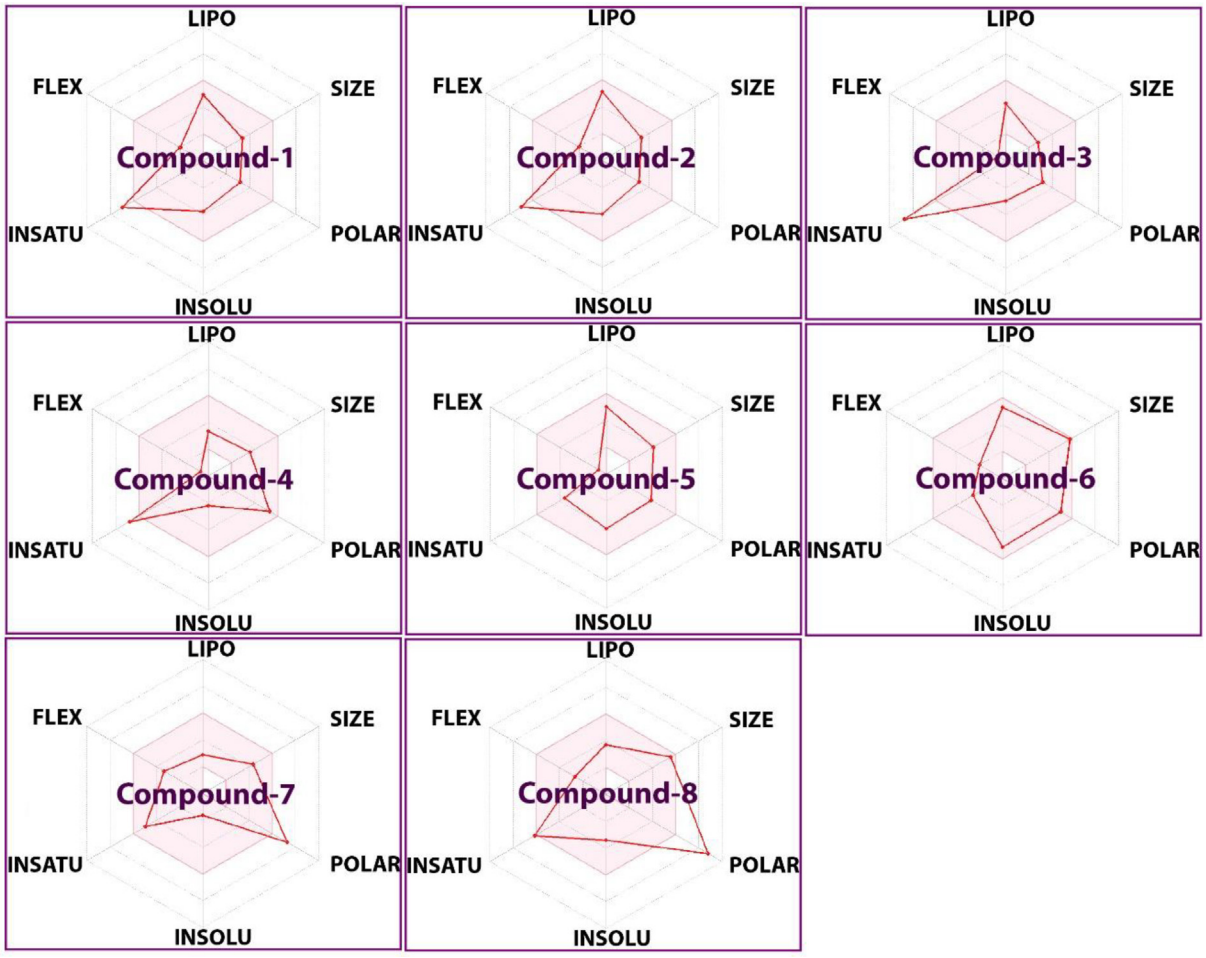

Fig. 12 *In-silico* pharmacokinetic assessment of compounds C1-C8.

4. Conclusion

Upon examining the interactions of eight phytochemicals with the human ACE2 receptor, and the SARS-CoV-2 Mpro, spike protein targets, two phytochemicals (C-5 and C-8) were identified as the best binding ligands. These were further examined in MD simulation studies to determine the stability of the ligand–protein interactions. QSAR, pharmacokinetic and drug-likeness properties studies revealed that C-5 may be the best candidate for the design and development of new drugs. Further studies are warranted to examine the potential of this phytochemical in the fight against COVID-19.

Author contributions

All data were generated in-house, and no paper mill was used. All authors agree to be accountable for all aspects of work ensuring integrity and accuracy.

CRediT authorship contribution statement

Mohnad Abdalla: Software, Visualization, Formal analysis. **Ranjan K. Mohapatra:** Conceptualization, Writing - original draft. **Ashish K. Sarangi:** Formal analysis. **Pranab K. Mohapatra:** Formal analysis. **Amr Ahmed El-Arabey:** Writing - review & editing. **Veronique Seidel:** Review and editing. **Mohammad Azam:** Validation, Review and editing. **Saud I. Al-Resayes:** Review. **Kuldeep Dhama:** Writing - review & editing. **Mahboob Alam:** Review. **Wafa Ali Eltayb:** Formal analysis.

Declaration of Competing Interest

The authors declare that they have no known competing financial interests or personal relationships that could have appeared to influence the work reported in this paper.

Acknowledgments

The authors acknowledge financial support through Researchers Supporting Project number (RSP-2021/147), King Saud University, Riyadh, Saudi Arabia. Dr. Mohnad Abdalla thanks Shandong University postdoctoral fellowship for the support. All the authors are thankful to their respective Institutions for their support.

Appendix A. Supplementary data

Supplementary data to this article can be found online at https://doi.org/10.1016/j.jscs.2021.101367.

References

[1] R.K. Mohapatra, P.K. Das, V. Kandi, Diab. Metab. Syndr. Clin. Res. Rev. 14 (2020) 1593–1594.
[2] R.K. Mohapatra, L. Pintilie, V. Kandi, A.K. Sarangi, D. Das, R. Sahu, L. Perekhoda, Chem. Biol. Drug Des. 96 (2020) 1187–1208.
[3] R.K. Mohapatra, S. Mishra, M. Azam, K. Dhama, Open Med. 16 (2021) 491–493.
[4] R.K. Mohapatra, M. Rahman, Anti-Infect. Agents 19 (4) (2021) 1–2.
[5] R.K. Mohapatra, P.K. Das, L. Pintilie, K. Dhama, Egypt. J. Basic Appl. Sci. 8 (1) (2021) 75–80.
[6] J.-F.-W. Chan, S. Yuan, K.-H. Kok, K.-K.-W. To, H. Chu, J. Yang, F. Xing, J. Liu, C.-C.-Y. Yip, R.-W.-S. Poon, H.-W. Tsoi, S.-K.-F. Lo, K.-H. Chan, V.-K.-M. Poon, W.-M. Chan, J.D. Ip, J.-P. Cai, V.-C.-C. Cheng, H. Chen, C.-K.-M. Hui, K.-Y. Yuen, Lancet 395 (10223) (2020) 514–523.
[7] K. Dhama, S.K. Patel, M. Pathak, M.I. Yatoo, R. Tiwari, Y.S. Malik, R.R. Singh, R. Sah, A.A. Rabaan, D.K. Bonilla-Aldana, A. J. Rodriguez-Morales, Travel Med. Infect. Dis. 37 (2020) 101755.
[8] C. McCarthy, C.P. O'Donnell, N.E.W. Kelly, D. O'Shea, A.E. Hog, Lancet 9 (2021) 445–447.
[9] B.M. Popkin, S. Du, W.D. Green, M.A. Beck, T. Algaith, C.H. Herbst, R.F. Alsukait, M. Alluhidan, N. Alazemi, M. Shekar, Obes. Rev. 21 (2020) e13128.
[10] I. Lega, L. Nistico, L. Palmieri, E. Caroppo, C.L. Noce, C. Donfrancesco, N. Vanacore, M.L. Scattoni, A. Picardi, A. Gigantesco, S. Brusaferro, G. Onderthe Italian National Institute of Health COVID-19 Mortality Group, E Clinical Medicine 35 (2021) 100854.
[11] R. Sah, A.P. Khatiwada, S. Shrestha, K.C. Bhuvan, R. Tiwari, R.K. Mohapatra, K. Dhama, A.J. Rodriguez-Morales, Travel Med. Infect. Dis. 41 (2021) 102037.
[12] R.K. Mohapatra, K. Dhama, A.A. El-Arabey, A.K. Sarangi, R. Tiwari, T.B. Emran, M. Azam, S.I. Al-Resayes, M.K. Raval, V. Seidel, M. Abdalla, J. King Saud Univ. Sci. (2021).
[13] L. Zhang, D. Lin, X. Sun, U. Curth, C. Drosten, L. Sauerhering, S. Becker, K. Rox, R. Hilgenfeld, Science 368 (6489) (2020) 409–412.
[14] Z. Jin, Y. Zhao, Y. Sun, B. Zhang, H. Wang, Y. Wu, Y. Zhu, C. Zhu, T. Hu, X. Du, Y. Duan, J. Yu, X. Yang, X. Yang, K. Yang, X. Liu, L.W. Guddat, G. Xiao, L. Zhang, H. Yang, Z. Rao, Nat. Struct. Mol. Biol. 27 (6) (2020) 529–532.
[15] C. Shivanika, S.D. Kumar, V. Ragunathan, P. Tiwari, A. Sumitha, P.B. Devi, J. Biomol. Struct. Dyn. (2020), https://doi.org/10.1080/07391102.2020.1815584.
[16] R.K. Mohapatra, L. Perekhoda, M. Azam, M. Suleiman, A.K. Sarangi, A. Semenets, L. Pintilie, S.I. Al-Resayes, J. King Saud Univ. Sci. 33 (2021) 101315.
[17] K. Baby, S. Maity, C.H. Mehta, A. Suresh, U.Y. Nayak, Y. Nayak, Arch. Med. Res. (2020) 1–10.
[18] R. Ghosh, A. Chakraborty, A. Biswas, S. Chowdhuri, J. Biomol. Struct. Dyn. (2020), https://doi.org/10.1080/07391102.2020.1841680.
[19] T. Joshi, T. Joshi, P. Sharma, S. Mathpal, H. Pundir, V. Bhatt, S. Chandra, Eur. Rev. Med. Pharmacol. Sci. 24 (8) (2020) 4529–4536.
[20] S.A. Lakshmi, R.M.B. Shafreen, A. Priya, K.P. Shunmugiah, J. Biomol. Struct. Dynam., (2020) 10.1080/07391102.2020.1778537.
[21] Ş. Adem, V. Eyupoglu, I. Sarfraz, A. Rasul, A.F. Zahoor, M. Ali, M. Abdalla, I.M. Ibrahim, A.A. Elfiky, Phytomedicine (2020), https://doi.org/10.1016/j.phymed.2020.153310.
[22] GaussView 6.0, 2019, Gaussian Inc., Wallingford, CT, USA, 2019.
[23] M.J. Frisch, GAUSIAN 09, Gaussian Inc., Wallingford CT, 2009.
[24] R.K. Mohapatra, M.M. El-ajaily, F.S. Alassbaly, A.K. Sarangi, D. Das, A.A. Maihub, S.F. Ben-Gweirif, A. Mahal, M. Suleiman, L. Perekhoda, M. Azam, T.H. Al-Noor, Chem. Pap. 75 (2021) 1005–1019.
[25] Schrodinger Release 2020-1, 2020, Glide, phase, ligprep. Schrodinger, LLC.
[26] F.D. Proft, P. Geerlings, Chem. Rev. 101 (2001) 1451–1464.
[27] G.E. Scuseria, J. Chem. Phys. 97 (1992) 7528–7530.
[28] T.A. Yousef, G.M.A. El-Reash, T.H. Rakha, U. El-Ayaan, Spectrochim Acta A 83 (1) (2011) 271–278.
[29] T.A. Yousef, T.H. Rakha, U. El-Ayaan, G.M.A. El-Reash, J. Mol. Struct. 1007 (2012) 146–157.
[30] A.K. Sarangi, B.B. Mahapatra, R.K. Mohapatra, S.K. Sethy, D. Das, L. Pintilie, K.-E-. Zahan, M. Azam, H. Meher, Appl. Organomet. Chem. 34 (2020) e5693.
[31] A.K. Sarangi, B.B. Mahapatra, S.K. Sethy, Chem. Afr. 1 (2018) 17–28.
[32] M.M. El-ajaily, A.K. Sarangi, R.K. Mohapatra, S.S. Hassan, R. N. Eldaghare, P.K. Mohapatra, M.K. Raval, D. Das, A. Mahal, A. Cipurkovic, T.H. Al-Noor, Chemistry Select 4 (34) (2019) 9999–10005.
[33] B.B. Mahapatra, R.R. Mishra, A.K. Sarangi, J. Saudi Chem. Soc. 20 (6) (2016) 635–643.
[34] T.A. Yousef, G.M. Abu El-Reash, R.M. El Morshedy, Polyhedron 45 (2012) 71–85.
[35] M. Govindarajan, S. Periandy, K. Carthigayen, Spectrochim Acta A 97 (2012) 411–422.
[36] R.G. Pearson, J. Org. Chem. 54 (6) (1989) 1423–1430.
[37] J. Padmanabhan, R. Parthasarathi, V. Subramanian, P. Chattaraj, J. Phys. Chem. 109 (48) (2005) 11043–11049.
[38] W. Radchatawedchakoon, S. Bamrungsuk, S. Namwijit, N. Apiratikul, U. Sakee, B. Yingyongnarongkul, Nat. Prod. Commun. 10 (11) (2015) 1973–1975.
[39] R. Kumar, S. Mehta, S.R. Pathak, Synth. Med. Agents Plants (2018) 75–103, https://doi.org/10.1016/B978-0-08-102071-5.00004-0.
[40] P.K. Mohapatra, K.S. Chopdar, G.C. Dash, M.K. Raval, Preprint, (2020) DOI: 10.26434/chemrxiv.12599915.
[41] S. Pant, M. Singh, V. Ravichandiran, U.S. Murty, H.K. Srivastava, J. Biomol. Struct. Dyn. (2020) 1–10.
[42] S. Beura, P. Chetti, J. Bimol. Struct. Dyn. (2020), https://doi.org/10.1080/07391102.2020.1772111.
[43] B. Dariya, G.P. Nagaraju, Cytokine Growth Factor Rev. (2020), https://doi.org/10.1016/j.cytogfr.2020.05.001.
[44] R.U. Savale, S. Bhowmick, S.M. Osman, F.A. Alasmary, T.M. Almutairi, D.S. Abdullah, P.C. Patil, M.A. Islam, Arch. Biochem. Biophys. 700 (2021) 108771.
[45] C.A. Lipinski, J. Pharmacol. Toxicol. Methods 44 (1) (2000) 235–249.
[46] C.A. Lipinski, Drug Disc. Today Technol. 1 (4) (2004) 337–341.